Oil-based mud waste reclamation and utilisation in low-density polyethylene composites

Siddique, Shohel; Yates, Kyari; Matthews, Kerr; Csetenyi, Laszlo J.; Njuguna, James

Published in:
Waste Management & Research

DOI:
10.1177/0734242X20941076

Publication date:
2020

Document Version
Peer reviewed version

Oil-based Mud Waste Reclamation and Utilisation in Low Density Polyethylene (LDPE) Composites

Shohel Siddique[1], Kyari Yates[2], Kerr Matthews[2], Laszlo J Csetenyi[3] and James Njuguna[1*]

[1]Centre for Advanced Engineering Materials, School of Engineering, Robert Gordon University, Riverside East, Garthdee Road, Aberdeen, AB10 7GJ, UK

[2]School of Pharmacy and Life Sciences, Robert Gordon University, Aberdeen, AB10 7GJ, UK

[2]School of Science and Engineering, University of Dundee, Dundee, DD1 4HN, UK

[*]*Corresponding Author Email : j.njuguna@rgu.ac.uk; Tel. +44 (0) 1224262304*

Abstract

Oil based mud (OBM) waste from oil and gas exploration industry can be valorised to tailor-made reclaimed clay reinforced low density polyethylene nanocomposites. This study aims to fill the information gap in the literature and to provide opportunities to explore the effective recovery and recycling techniques of the resources present in OBM waste stream. The elemental analysis using Inductively coupled plasma - optical emission spectrometry

Siddique, S., Yates, K., Matthews, K., Csetenyi, L.J. & Njuguna, J. 'Oil-based mud waste reclamation and utilisation in low-density polyethylene composites', *Waste Management & Research*. © 2020 The Authors. DOI: 10.1177/0734242X20941076.

(ICP-OES) and X-Ray Fluorescence (XRF) analyses, chemical structural analysis by FTIR and morphological analysis of LDPE/MMT and LDPE/OBM slurry nanocomposites by SEM have been conducted. Further analysis including calorimetry, thermogravimetry, spectroscopy, microscopy, energy dispersive X-ray analysis (EDXA) and X-ray diffraction was carried out to evaluate the thermo-chemical characteristics of OBM waste and OBM clay reinforced LDPE nanocomposites, confirming the presence of different clay minerals including inorganic salts in OBM slurry powder. The microscopic analysis revealed that the distance between polymer matrix and OBM slurry filler is lesser than that of MMT which suggests better interfacial adhesion of OBM slurry compared to the adhesion between MMT and LDPE matrix. This was also confirmed by XRD analysis which showed the superior delamination structure OBM slurry compared to the structure of MMT. There is a trend noticeable for both of these fillers that the nanocomposites with higher percentage filler contents (7.5 and 10.0 wt% in this case) indicated to act as a thermal conductive material. The heat capacity values of nanocomposites decreased about 33% in LDPE with 7.5 wt% MMT and about 17% in LDPE with 10.0 wt% OBM slurry. It is also noticeable, for both nanocomposites that the residue remaining after 1000° C increases with the incremental wt% of fillers in nanocomposites. There is a big difference in residue amount (in %) left after TGA in two nanocomposites indicates OBM slurry may have significant influence in decomposing LDPE matrix which might be an interesting area to explore in the future. The results provide insight and opportunity to manufacture waste-derived renewable nanocomposites with enhanced structural and thermal properties.

Keywords: oil-based mud, resource recovery waste characterisation, polymer nanocomposites, thermal degradation study.

Introduction

Sustainable waste management in oil and gas industries represents the rational recovery or uses of resources, ensure health and safety and thus improvement of life quality, protection of eco-systems and to convert waste into valuable products (Elektorowicz and Habibi, 2005; Maloney and Yoxtheimer, 2012; Colborn *et al*., 2011; Binnemans *et al*., 2015). Spent drilling fluids, also known as mud predominantly oil based mud (OBM) is one of the main source of waste stream in oil and gas industry (Onwukwe and Nwakaudu, 2012; Hickenbottom *et al*., 2013; Susich and Schwenne, 2004; Ismail *et al*., 2017). A drilling fluid is an essential part of drilling operation in oil and gas exploration operation to perform several functions such as removing and cleaning drill cuttings from the downhole, cooling and lubricating the drill bit, controlling the hydraulic pressure to protect well blowouts (Caenn *et al*., 2011; Fink 2015; Khodja *et al*., 2010). Although OBM is environmentally hazardous, but due to its special features such as reliable shale inhibition, excellent lubricity, OBM is still an essential part of deep drilling in oil and gas exploration industries (Zhong *et al*., 2011; Liu *et al*., 2004 and Gholami *et al*., 2018;). This deep drilling operation intensifies the pollutants addition in OBM which is considered a big concern for different stakeholders including spent

OBM waste treatment services, local authorities, environmental activists and regulators involved in running waste framework directives (Veil, 2002 and Force, 2009;).

To protect the environment and to recycle or to recover the useful compounds associated with this waste stream, different techniques have been applied in drilling fluid waste treatment operation including, solidification technology (Tuncan *et al*., 2000), the solid-liquid separation technology (Zou *et al*., 2011), MTC (mud transform to cement) technology (Nahm and Wyant, 1993), incineration technology (Onwukwe and Nwakaudu, 2012) and some other thermo-mechanical treatments (Mokhalalati *et al*., 2000). These processes have certain advantages and disadvantages in respect to operational or treatment time, cost, space requirement and treatment efficiency. However, these processes are successful in protecting environment in some extent, but the detrimental effects of this waste on the environment are common and raising in concerning level (Ball *et al*., 2012). The management of OBM waste is an important issue since most of the hazardous chemicals associated with OBM waste exist, even in solid form which are disposed of in landfill sites (Walter *et al*., 2012; Hainey *et al*., 1999). Interestingly, this OBM waste contains significant amounts of clay minerals and metals which attract the use of this waste in engineering polymeric nanocomposites applications (Siddique *et al*., 2019a; Siddique *et al*., 2019b).

An in depth qualitative analysis of petroleum sludge was performed by Andrade *et al*. (2009). The key findings from the study confirmed the presence of irregular sizes of dry oily petroleum sludge by Scanning Electron Microscopy (SEM) analysis. Moreover, smaller sized layered platelets were

also highlighted in that study which is attributed to bentonite clay. The existing larger particles in dry oily petroleum sludge are suggested to be barite, calcite, sandstone and quartz which were manifested by the findings from other study performed by Wang *et al*., (2012) and Bin Merdhah (2010). Another research group presented different minerals content in petroleum sludge by XRD and ATR-FTIR analysis. The XRD pattern in that study at certain peaks at 2-theta data confirmed the presence of barite (2θ = 26.2°(26°), 29.1°(29°), 31.9° and 43.5°), quartz (2θ = 21.5, 23 and 26.0°), zinc oxide (30-40°), montmorillonite (6°, 9°, 12°, 14°, 18°, 27°, 30°, 61°), bentonite (6°, 9°, 12°, 14.8°, 18°, 27°, 30°, 61°), Magnetite oxide (35.5°) and calcite (29.6°, 39°). such as (2θ = 26.2°(26°), 29.1°(29°), 31.9° and 43.5°). In addition, the band peaks at 1166 cm^{-1} in their ATR-FTIR study also confirmed the presence of Si-O stretching of quartz and the spectra bands at 1124 cm^{-1} and 1014 cm^{-1} highlighted the presence of montmorillonite (Pendleton, 2014).

Several research groups have reported the thermal stability behaviour of polyethylene clay nanocomposites in different research articles. Xie *et al*. (2012) have reported the thermal stability by analysing the TGA curves (under a nitrogen gas condition) of their LDPE/OMMT nanocomposite specimens. The onset degradation temperature of the nanocomposite specimens of only 0.5 wt% have increased by a considerable 23 °C for OMMT compared to that of neat LDPE. Morawiec *et al*. (2005) have also performed thermogravimetric analysis on their samples (TGA) which were conducted in a nitrogen atmosphere and in an air atmosphere. Based on the TGA curves, Morawiec *et al*. (2005) have concluded that the presence of filler did not significantly improve the thermal stability in a nitrogen atmosphere since decomposition

temperature and peak intensity have all been recorded to be relatively consistent. More research on the thermal properties of organoclay/polymer nanocomposites carried out by Attaran *et al*. (2015) have reported no notable change in the nucleation activity between neat LDPE and LDPE/OMMT 6 wt% specimens from their DSC analysis. Hemati *et al*. (2011) have observed improved thermal stability of their LDPE/LLDPE/nanocomposites in the air and nitrogen atmosphere and observed a weight loss at a lower temperature due to the decomposition of the organic modifier.

The amount of total petroleum hydrocarbon (TPH) associated with OBM waste is the key factor in handling OBM waste in oil and gas industry due to the restriction of disposing OBM waste containing more than 1% oil on residue (Perry and Griffin, 2001). Perry and Griffin (2001) identified the TPH content in OBM and associated drill cuttings by using gas chromatography which was 65,000 ppm. Furthermore, particle size analysis results were also presented in that study and the average particles was 210 µm by using sieve method reported in that study. Although the study by Perry and Griffin (2001) presented some characterisation of the OBM waste, but this study was limited to identify the nanoparticles content of the OBM waste. However, Gbadebo and Taiwo *et al*. (2010) investigated the elements presents in both oil based and water based mud using atomic absorbtion spectrophotometry and the content of Fe, Ca, Mg, Cr, Pb, Mn and Ni were reported in that study. Another study performed by Adegbotolu *et al*. (2014) also highlighted the presence of heavy and trace metals using ICPOES analysis of oil-based drilling fluid and cuttings. To investigate the utilization of these clay minerals including metals as nanofiller in polymer matrix to improve thermal stability is an interesting

area of research performed at Centre for Advanced Engineering Materials, Robert Gordon University.

The OBM waste slurry is generally composed of clay minerals including metals in a strong suspended solid phase condition. This suspended clay slurry has been selected in this study as reinforcement in LDPE matrix not only because it improves the thermal stability, but in an aspect of valorising an unwanted and unexploited waste discarded at landfill site as an existing practice in oil and gas industry. This article highlights other properties of OBM waste and delivers the potential opportunity of utilising this OBM waste as nanofiller in developing and manufacturing novel nanocomposite materials.

Materials and experimental details

Materials and samples preparation

The OBM waste slurry was donated by a local oil and gas service company in Aberdeen, UK. To characterise the solid content in this OBM slurry and to use this OBM powder as filler in nanocomposite, the petroleum hydrocarbon were eliminated by using thermal treatment process. To obtain the solid residue, the OBM slurry is heated sporadically by following the stages: 50°C for 12 hours (1st heating) followed by 80°C for a further 12 hours (2nd heating); finally the residue is heated at 700°C for 12 hours (3rd heating). To facilitate to carry out different analysis and use as a filler in nanocomposite manufacturing, this solid residue was crushed into smaller pieces using a grinder followed by a further size reduction to produce powder by using IKA UltraTurrax ball mill.

Lupolen 1800S (trade name of LDPE, manufactured by Lyondellbasell industries Ltd) was supplied by Northern Polymers and Plastics Ltd, UK. It has a melting point of 106°C and a V-2 rating in accordance to UL 94 (vertical burning test) at 1.6 mm thickness. The montmorillonite (MMT), K10 was supplied by Sigma-Aldrich, UK which used as a reference material to evaluate characteristics between MMT and OBM nanofiller. Montmorillonite was chosen for its established and typical use as filler in polymer compounds.

LDPE/OBM slurry and LDPE/MMT nanocomposite manufacturing process

LDPE/OBM slurry and LDPE/MMT nanocomposites were manufactured by reinforcing fillers in certain weight percentages in LDPE matrix such as 2.5, 5.0, 7.5 and 10.0 wt% in this study. LDPE pellets and MMT were dried at 90°C overnight prior to melt compounding. Moisture free LDPE (oven dried at 90°C for 12 hours) mixed with slurry prior to melt compounding. LDPE/OBM slurry and LDPE/MMT mixed compounds containing different weight percentage of fillers were manufactured using twin screw extruder (TwinTech extrusion Ltd.) at 60 rpm over five different heating zones: 1st zone (120°C), 2nd zone (200°C), 3rd zone (210°C), 4th zone (200°C) and die/5th zone (200°C). The compounded strands were prepared into pellets by using a pelletiser which were then injection moulded into a bar mould (dual cavity) using the barrel temperature at 230°C with a moulding pressure of 10 bar to manufacture nanocomposite materials for different analyses.

Characterisation

Scanning electron microscope (SEM) was performed using a JEOL JSM-7400F instrument with a magnification of 25000X, 8.0 mm working distance (WD) and accelerating potential of 5.0 kV. The samples were coated with gold and palladium using sputter deposition for 2 minutes prior to the analysis.

Attenuated Total Reflectance- Fourier Transform Infrared (FTIR) Spectroscopy was carried out for 32 scans between 4000-400 cm^{-1} with a resolution of 4 cm^{-1}. A blank measurement was taken to minimise the influence of water vapour and carbon dioxide from the atmosphere. The air background was collected and then the sample spectra was collected and saved. The dry drilling waste sample was placed between the ATR stage and the diamond.

Mineralogical composition for both OBM powder, MMT and LDPE/OBMFs nanocomposites was determined by X-ray diffraction (XRD) using a Siemens D5000 diffractometer with Cu Kα radiation (λ = 0.15406 nm) in the range of 3-60° and 0.1° 2θ step size and scanning speed was 0.02°s^{-1}. the diffraction details and relative intensities were obtained and compared by using Rietveld refinement software.

Element analysis

To determine the elemental composition of dry OBM waste, LDPE/OBM slurry nanocomposites and LDPE/MMT nanocomposites, energy dispersive x-ray analysis (EDXA) (Oxford Instruments INCA Energy) was carried out. To determine the inorganic elements including heavy metals exist in dry OBM slurry powder, LDPE/MMT and LDPE/OBM slurry nanocomposites, an investigation carried out using Malvern Panalytical XRF spectrometers.

Thermal analysis

TA Q100 instrument under a nitrogen environment was used for performing Differential Scanning Calorimetry (DSC) thermal analysis by following heat-cool-heat procedure with the temperature ramp of 10°C/min from -20°C to 250°C. The TA Q500 instrument was used to perform Thermogravimetric Analysis (TGA) to identify the degradation and decomposition nature of the materials. The temperature was set on ramp mode from room temperature (15°C) to 1000°C at a rate of 10°C/minute.

Result and discussion

Morphology study

In Fig. 1, the micrograph shows the tightly stacked platelets of montmorillonite and OBM waste powder with size ranges up to 1000nm.

[Fig. 1]

The SEM micrographs were used to investigate the morphological representation of different clay minerals present in OBM waste which is compared with that of standard montmorillonite sample supplied by Sigma-Aldrich. Both micrographs represent the platelet structure. However OBM shows tightly stacked the platelets with variant sizes of platelets with different shapes whereas montmorillonite shows regular platelet shapes with uniform

structure. It can articulate here that different clay minerals may influence the structure and shape of the platelets present in OBM waste.

[Fig. 2] [Fig. 3]

To identify the surface topography of reclaimed clay from oil based mud waste reinforced LDPE nanocomposites, montmorillonite reinforced LDPE nanocomposites are considered as a standard benchmark samples. It is noticeable that the OBM clay platelets are better distributed in polymer matrix compare to MMT clay platelets are distributed in LDPE matrix. The interfacial adhesion between clay platelets and polymer matrix is stronger in LDPE/OBM slurry nanocomposites compare to the adhesion between montmorillonite and LDPE matrix. This is predominantly noticeable in samples with higher filler content such as LDPE with 7.5 and 10.0 wt% filler nanocomposites show strong physical contact between filler and polymer matrix. From the morphological observation it can be concluded here that OBM slurry is distributed evenly throughout the polymer matrix and following the regular gap between platelets in LDPE with 2.5, 5.0 and 7.5 wt% OBM slurry nanocomposites. It can be highlighted here that the interfacial gap between platelets and LDPE matrix is lesser in LDPE/OBM slurry nanocomposites compare to that in LDPE/MMT nanocomposites. This observation leads to articulate the superior interfacial adhesion mechanism between OBM slurry and LDPE matrix compare to the adhesion mechanism in LDPE/MMT nanocomposites. it can be concluded here that OBM slurry is distributed

evenly throughout the polymer matrix and following the regular gap between platelets in LDPE with 2.5, 5 and 7.5 wt.% OBM slurry nanocomposites.

Chemical structure analysis

The ATR-FTIR spectrum analysis of neat LDPE, LDPE/MMT nanocomposites and LDPE/OBM slurry nanocomposites have been carried out and the resulting spectra are presented in Fig. 4 and 5.

[Fig.4] [Fig.5]

The absorption bands due to structural OH and Si-O groups play an important role to identify different clay minerals present in LDPE/OBM slurry and LDPE/MMT nanocomposites. The chemical structure of LDPE and LDPE/MMT nanocomposites were identified by using ATR-FTIR which represents the IR transmittance peaks at 1053.29 cm^{-1} corresponding to montmorillonite in Fig. 4 (Madejova, 2003), (Nayak and Singh, 2007). In Fig. 5, there are three peaks at 2364.02 cm^{-1}, 1713.90 cm^{-1} and 1087.37 cm^{-1} are clearly noticeable. The presence of band at 2364.02 cm^{-1} indicates the possibility of the presence of illite (Nayak and Singh, 2007). The peak at 1087.37 cm^{-1} represents the stretching of Si-O which indicates the presence of Kaolinite (Siddique *et al*., 2019b) (Nayak and Singh, 2007). The infrared absorption band at 1713.90 cm^{-1} corresponds to silica-aluminium and aluminosilicates present in the nanocomposites (Djomgoue and Njopwouo, 2013).

Mineral composition analysis

Mineralogical analysis for OBM waste showed that it is essentially dominant by muscovite, barite, montmorillonite and quartz. However a trace amount of kaolinite, meionite, halloysite, aluminium, silicon chlorite and anorthite are also present in OBM waste.

[Fig. 6]

XRD patterns of OBM samples in air dried state were compared to the XRD pattern of montmorillonite as a reference which indicated the presence of sharp montmorillonite peaks in OBM waste. The diffraction peaks in Fig. 6 corresponded to the sets in the 29-1490 JCPDS card and confirmed the presence of montmorillonite by using Rietveld refinement software. The d_{001} spacing was calculated using Bragg's law $n\lambda = 2d \sin\theta$ where λ is the wavelength of X-ray radiation used in the analysis, *d* corresponds the distance between diffraction lattice planes and θ is the half diffraction angle. For MMT and OBM slurry waste a diffraction peak at about $2\theta = 6.700°$ was observed which corresponded to a *d*-spacing of 12.62 Å and 13.2Å respectively.

[Fig. 7] [Fig.8]

The XRD analyses are illustrated in Fig. 7 and Fig. 8 addressing the diffractograms at (a) wide angle X-ray diffraction (WAXD); and (b) small angle X-ray diffraction of LDPE/MMT and LDPE/OBM slurry nanocomposites

respectively. In Fig. 7, XRD patterns of LDPE and LDPE/MMT nanocomposites are presented. A clear shift of the diffraction peaks of the planes (001) of MMT towards lower angles for the LDPE/MMT nanocomposites is noted. The basal spacing of MMT increases with different nanocomposites in different ratios. Using Bragg's law $n\lambda = 2d\sin\theta$, where λ is the wavelength of the X-ray radiation applied in the experiment, *d* corresponds to the distance between diffraction lattice plane and θ is the half of the diffraction angle.

The diffraction peak of MMT was observed at 2θ = 11.40° which corresponds to a *d*-spacing of 7.75 Å. The *d*-spacings of LDPE with 2.5 wt% and 5.0 wt% MMT nanocomposites were identified at 10.6° and 10.2° which corresponds to the value of 8.34 Å and 8.67 Å, respectively. However, the *d*-spacings of LDPE with 7.5 wt% and 10.0 wt% MMT nanocomposites were analysed at 9.3° and 8.6° which corresponds to the value of 9.50 Å and 10.27 Å, respectively. Moreover, the diffraction peak of OBM slurry (dry powder) was observed at 2θ = 12.40° which corresponds to a *d*-spacing of 7.13 Å. The *d*-spacings of LDPE with 2.5 wt% and 5.0 wt% OBM slurry nanocomposites were identified at 10.9° and 9.7° which corresponds to the value of 8.11 Å and 9.11 Å, respectively. However, the *d*-spacings of LDPE with 7.5 wt% and 10.0 wt% OBM slurry nanocomposites were identified at 9.1° and 8.2° which corresponds to the value of 9.71 Å and 10.77 Å, respectively. Considering the XRD data obtained in this investigation, it can be inferred that OBM slurry showed better delamination (higher basal spacing) compare to that of MMT in LDPE matrix.

Elemental analysis

EDXA was carried out to determine the elemental composition of dry OBM waste, neat LDPE, LDPE/MMT and LDPE/OBM slurry nanocomposites which is presented in Table 1.

[Table 1]

The XRF chemical composition of OBM slurry powder, neat LDPE, LDPE/MMT and LDPE/OBM slurry nanocomposites is presented in Table 2.

[Table 2]

XRF analysis confirmed that $BaSO_4$, SiO_2, Al_2O_3, CaO and Fe_2O_3 were found to be major constituents of OBM slurry (dry powder). Silicon dioxides, iron oxides, alumina, barium sulphate, calcium and manganese oxides are known to be the hardest substances. The presence of these hard substances in OBM powder suggested that this slurry can be used as a particulate reinforcement in polymer matrix.

Thermal properties

To investigate the thermal degradation behaviour of OBM waste, non-isothermal measurements were taken by using DSC instrument and the results are shown in Fig.9.

[Fig. 9]

Comparing different thermograms in Fig. 9 (b) there are two peaks present in melting temperature at 56.64°C and 59.05°C. It can be attributed here that the first peak at 56.64°C corresponds to the γ crystal phase whereas the peak at 59.05°C is the representative of α phase crystals. It is important to notice here that the crystal phase is dominant in this OBM waste which is thermodynamically stronger than γ phase crystals. This observation is also established by the amount of residue recovered after TGA study. Fig. 9 (a) and 9 (c) shows the glass transition temperature (Tg) and crystallisation temperature (Tc) of OBM waste respectively.

To identify the influence of OBM slurry on the thermal degradation behaviour of LDPE/OBM slurry nanocomposites, non-isothermal DSC studies were conducted. Investigation on the thermal degradation behaviour of LDPE/MMT nanocomposites considered as a benchmark standard.

[Fig. 10] [Fig. 11]

Analysing the DSC thermograms in Fig. 10a, it can be highlighted that there are not any significant changes in the glass transition temperature (Tg) of LDPE/MMT nanocomposite materials, but this Tg is lower than the Tg of neat LDPE. However, there are not any significant changes among the Tg of neat LDPE and LDPE/OBM slurry nanocomposites. The same trend is noticeable in comparing the thermograms between LDPE/MMT and LDPE/OBM slurry nanocomposites. The melting point remains almost same for neat LDPE and LDPE/OBM slurry nanocomposites whereas the addition of MMT filler lowered

the melting point of LDPE/MMT nanocomposites. Considering the heat capacity value from the melting thermograms in Fig. 10 and Fig. 11, the % of crystallinity can be identified using the following equation:

$$\% \text{ of crystallinity} = [\Delta Hm - \Delta Hc] / \Delta Hm^0 * 100\% \quad (1)$$

Where ΔHm is the heat of melting, ΔHc the heat of cold crystallisation which is 0 in this experiment (ΔHc=0 in this case) due to the absence of cold crystallisation phase in this experiment, and ΔHm° is a reference value if the polymer were 100% crystalline. All the units are in J/g and the value of ΔHm° is 293 Jg^{-1} (Siddique *et al*., 2019b). The % of crystallinity value of LDPE, LDPE/MMT and LDPE/OBM slurry nanocomposites are presented in Table 3.

[Table 3]

It is noticeable that there is a decreasing trend of % of crystallinity in nanocomposites with higher (more than 5.0 wt%) filler contents. However, there is an indication of increasing % of crystallinity in nanocomposites with lower (less than 5.0 wt%) filler contents. This decreasing trend in nanocomposites with higher wt% filler contents can be explained by the interruption caused by this filler in LDPE matrix, which hinders the motion of the polymer chain segments and inhibit crystal growth.

The specific heat capacity value of LDPE, LDPE/MMT and LDPE/OBM slurry nanocomposites have been identified by analysing the thermograms in Fig. 10(c) and 11(c). The specific heat capacity value can be determined by the following equations:

$$C_p = (\delta Q / \delta T) \quad (2)$$

$C_p = (\delta Q / \delta t) \times (\delta t / \delta T)$ (3)

Where *Cp* is the heat capacity in Joules per Kelvin (JK^{-1}), Q is heat energy in Joule and T is the temperature denoted as °C or K. *δQ/δt* represents the heat flow and *δt/δT* corresponds to reciprocal heating rate (Siddique *et al*., 2019a). By using these two equations, the analysed specific heat capacities of neat LDPE, LDPE/MMT and LDPE/OBM slurry nanocomposites are identified, as presented in Table 3.

The heat capacity data presented in Table 3 shows the negative effects of clay minerals as filler in polymer matrix. However, LDPE with lower filler contents (2.5 and 5.0 wt%) showed higher specific heat capacity tendency compare to that of higher filler contents nanocomposites. There is a trend noticeable for both of these fillers that the nanocomposites with higher percentage filler contents (7.5 and 10.0 wt% in this case) indicated to act as a thermal conductive material. The heat capacity value decreases about 33% in LDPE with 7.5 wt% MMT nanocomposite whereas it is about 17% heat reduction in LDPE with 10.0 wt% OBM slurry nanocomposites.

It is important to identify the different phases exist in semi-crystalline polymer nanocomposites as this will dictate mechanical and thermal properties of the materials. Evaluating the heat capacity value, *Cp* in glass transition temperature, mobile amorphous fraction (MAF) can be identified by the following equation:

$MAF = \Delta C_p / \Delta C_{pamp}$ (4)

Where $\Delta C_p/\Delta C_{p\ amp}$ are the heat capacity increments at the glass transition temperature of LDPE and its nanocomposites and the pure amorphous LDPE

polymer, respectively. Using the MAF value, rigid amorphous fraction (RAF) can also be identified by the following equation:

$$RAF = 1 - crystallinity - \Delta C_p / \Delta C_{p\,amp} \quad (5)$$

Using the equations (4) and (5), the MAF and RAF values are identified and presented in Table 3.

It can be highlighted here that the RAF increases up to five times compare to RAF of neat LDPE by adding MMT fillers in LDPE matrix. There is an increasing trend of RAF noticeable with the increasing amount of MMT content in LDPE/MMT nanocomposites. However, the RAF increases about three times compare to the RAF of neat LDPE by adding OBM slurry in LDPE matrix. The RAF remains almost constant for different LDPE/OBM slurry nanocomposites which indicate there is no influence of filler amounts increasing the RAF in LDPE/OBM slurry nanocomposites.

The thermal degradation of OBM waste has been analysed in N_2 environment using TA instrument TGA Q500. Onset degradation of the sample in different stages is presented in Fig. 12.

[Fig. 12]

Fig. 12 (a), 12 (b) and 12 (c) shows the onset degradation of OBM waste at different stages such as 5%, 10% and 65% weight loss respectively. Fig. 12 (d) shows the weight % of residue left after 1000°C. Since this OBM waste is a complex mix of organic and inorganic substances, the thermograms associated with the endothermic reaction of any specific materials/minerals is

very difficult to establish. However Table 4 shows the potential thermograms peaks associated with different clay minerals.

[Table 4]

Thermal degradation behaviour of LDPE/MMT and LDPE/OBM slurry nanocomposites has been studied under the same environmental condition and analysis method as the environmental condition and analysis method followed in identifying the thermal degradation behaviour of OBM slurry waste.

[Fig. 13] [Fig. 14]

The degradation scenario of these materials at different heating stages are analysed and the key findings are presented in Table 5.

[Table 5]

The onset degradation temperature of neat LDPE, LDPE/MMT and LDPE/OBM slurry nanocomposites materials are presented at weight % losses of 5% and 10%. In all cases, the onset degradation temperature of nanocomposites is less than that of neat LDPE. There are not any significant changes in D1/2 time (the time needed to reach 50% degradation) which indicates the filler content may not have any influence on degradation time and the increase in filler contents in nanocomposites may intensify the heat flow which is shown elevated temperature in D1/2 time. It is also noticeable,

for both nanocomposites, the residue remains after 1000° C increases with the incremental wt% of fillers in nanocomposites. There is a big difference in residue amount (in %) left after TGA in two nanocomposites indicates OBM slurry may have significant influence in decomposing LDPE matrix which might be an interesting area to explore in the future.

Conclusions

The possibility of manufacturing novel economically valuable engineering nanocomposite materials from OBM waste has been demonstrated. Findings from different characterisation including morphology study, chemical and mineralogical study and thermal study it can be concluded that this waste is associated with critical raw materials for different industrial applications, environmentally significant materials including heavy metals and potentially nanoclay as a green filler in nanocomposite manufacturing to improve mechanical, thermal, gas barrier and flame-retardant properties.

In concluding remarks, it was highlighted based on the analyses results that OBM clay can be dispersed evenly compared to MMT in LDPE polymer. Furthermore, there is not any significant new peaks were apparent in FTIR analysis which confirmed the OBM clay minerals masked with the LDPE polymer chains reflecting the compatibility of OBM clay with LDPE. LDPE with higher wt% OBM slurry filler loadings (7.5 and 10 wt% in this study) behaved as a thermal conductive material based on the specific heat capacity data reported in this study. Considering different analyses results presented in this study it can be highlighted that this OBM waste can utilised sustainably which is now considered the environmental burden in the industry. The combined

initiative may lead to apply innovative technologies and approaches that may bring the sustainable OBM waste management practices in oil and gas industries. Practical applications of reclaimed clay from OBM waste in the area of engineering structural materials are currently under investigation in our laboratories as compared to those of commercial nanoparticles, with promising results for the utilisation of such clay minerals rich OBM waste stream in structural components in aerospace and automotive industry.

References

Adegbotolu UV, Njuguna J, Pollard P and Yates K (2014) Waste to Want: Polymer nanocomposites using nanoclays extracted from Oil based drilling mud waste. *IOP Conference Series: Materials Science and Engineering* IOP Publishing: 012023

Andrade PF, Azevedo TF, Gimenez IF, Souza FAG and Barreto LS (2009) Conductive carbon–clay nanocomposites from petroleum oily sludge. *Journal of hazardous materials* 167(1-3): 879-884.

Attaran SA, Hassan A and Wahit MU (2015) Effects of ENR and OMMT on barrier and tensile properties of LDPE nanocomposite film. *Iranian Polymer Journal* 24(5): 367-378.

Ball AS, Stewart RJ and Schliephake K (2012) A review of the current options for the treatment and safe disposal of drill cuttings. *Waste Management & Research* 30(5): 457-473.

Bin Merdhah A (2010) Inhibition of calcium sulfate and strontium sulfate scale in waterflood. *SPE Production & Operations* 25(04): 545-552.

Binnemans K, Jones PT, Blanpain B, Van Gerven T and Pontikes Y (2015) Towards zero-waste valorisation of rare-earth-containing industrial process residues: a critical review. *Journal of Cleaner Production* 99: 17-38.

Caenn R, Darley HC and Gray GR (2011) Composition and properties of drilling and completion fluids. *Gulf professional publishing*.

Colborn T, Kwiatkowski C, Schultz K and Bachran M (2011) Natural gas operations from a public health perspective. Human and ecological risk assessment: *An International Journal* 17(5):1039-1056.

Cranford PJ and Gordon DC (1991) Chronic sublethal impact of mineral oil-based drilling mud cuttings on adult sea scallops. *Marine Pollution Bulletin*, 22(7): 339-344.

Djomgoue P and Njopwouo D (2013) FT-IR spectroscopy applied for surface clays characterization. *Journal of Surface Engineered Materials and Advanced Technology* 3(04): 275.

Elektorowicz M and Habibi S (2005). Sustainable waste management: recovery of fuels from petroleum sludge. *Canadian Journal of Civil Engineering* 32(1):164-169.

FINK J (2015) Water-based chemicals and technology for drilling, completion, and workover fluids. *Gulf Professional Publishing*.

Force DFT (2009) Drilling fluids and health risk management. A guide for drilling personnel, managers and health professionals in the oil and gas industry. *OGP Report Number 396, International Petroleum Industry Environmental Conservation Association, International Association of Oil & Gas Producers*.

Gholami R, Elochukwu H, Fakhari N and Sarmadivaleh M (2018) A review on borehole instability in active shale formations: interactions, mechanisms and inhibitors. *Earth-science reviews*, 177: 2-13.

Hainey BW, Keck RG, Smith MB, Lynch KW and Barth JW (1999) On-site fracturing disposal of oilfield-waste solids in Wilmington field, California. *SPE production & facilities*, 14(02): 83-87.

Hemati F and Garmabi H (2011) Compatibilised LDPE/LLDPE/nanoclay nanocomposites: I. Structural, mechanical, and thermal properties. *The Canadian Journal of Chemical Engineering*, 89(1): 187-196.

Hickenbottom KL, Hancock NT, Hutchings NR, Appleton EW, Beaudry EG, Xu P and Cath TY (2013) Forward osmosis treatment of drilling mud and fracturing wastewater from oil and gas operations. *Desalination*, 312: 60-66.

Gbadebo A, Taiwo A and Eghele U (2010) Environmental impacts of drilling mud and cutting wastes from the Igbokoda onshore oil wells, Southwestern Nigeria. *Indian Journal of Science and Technology*, 3(5): 504-510.

Grim RE and Rowland RA (1942) Differential thermal analyses of clay minerals and other hydrous materials. *Report of investigations no.085*.

Ismail AR, Alias AH, Sulaiman WRW, Jaafar MZ and Ismail I (2017) Drilling fluid waste management in drilling for oil and gas wells. *Chemical Engineering Transactions*, 56: 1351-1356.

Khodja M, Canselier JP, Bergaya F, Fourar K, Khodja M, Cohaut N and Benmounah A (2010) Shale problems and water-based drilling fluid optimisation in the Hassi Messaoud Algerian oil field. *Applied Clay Science* 49(4): 383-393.

Liu S, Mo X, Zhang C, Sun D and Mu C (2004) Swelling inhibition by polyglycols in montmorillonite dispersions. *Journal of dispersion science and technology*, 25(1): 63-66.

Madejova J (2003) FTIR techniques in clay mineral studies. *Vibrational spectroscopy*, 31(1): 1-10.

Maloney KO and Yoxtheimer DA (2012) Production and disposal of waste materials from gas and oil extraction from the Marcellus Shale play in Pennsylvania. *Environmental Practice*, 14(4): 278-287.

Mokhalalati T, Al-Suwaidi A and Hendi AE (2000) Managing Onshore Drilling Wastes-Abu Dhabi Experience. *Abu Dhabi International Petroleum Exhibition and Conference. Society of Petroleum Engineers*.

Morawiec J, Pawlak A, Slouf M, Galeski A, Piorkowska E and Krasnikowa N (2005) Preparation and properties of compatibilized LDPE/organo-modified montmorillonite nanocomposites. *European Polymer Journal*, 41(5): 1115-1122.

Nahm JJ and Wyant RE Shell Oil Co (1993) Method for conversion of oil-base mud to oil mud-cement. *U.S. Patent* 5,213,160.

Nayak PS and Singh BK (2007) Instrumental characterization of clay by XRF, XRD and FTIR. *Bulletin of Materials Science*, 30(3): 235-238.

Onwukwe SI and Nwakaudu MS (2012). Drilling wastes generation and management approach. *International Journal of Environmental Science and Development*, 3(3): 252.

Pendleton SJ (2014) The migration of radioactive caesium and strontium through a bentonite-like clay (*Doctoral dissertation*, © Stephen James Pendleton).

Perry M and Griffin J (2001) Chemical Treatment of Cuttings Drilled With Oil-Based Mud Employing a Laboratory Simulated Soil Washing Procedure. *SPE/EPA/DOE Exploration and Production Environmental Conference*. Society of Petroleum Engineers.

Siddique S, Kwoffie L, Addae-Afoakwa, K, Yates K and Njuguna J (2019a) The crystallinity and thermal degradation behaviour of polyamide 6/Oil Based Mud Fillers (PA6/OBMFs) nanocomposites. *Polymer degradation and stability* 159: 139-152.

Siddique S, Smith GD, Yates K, Mishra AK, Matthews K, Csetenyi LJ and Njuguna J (2019b) Structural and thermal degradation behaviour of reclaimed clay nano-reinforced low-density polyethylene nanocomposites. *Journal of Polymer Research* 26(6): 154.

Susich ML and Schwenne MW (2004) January. Onshore drilling waste management: Beneficial reuse of cuttings. In *SPE International Conference on Health, Safety, and Environment in Oil and Gas Exploration and Production. Society of Petroleum Engineers*.

Tuncan A, Tuncan M and Koyuncu H (2000) Use of petroleum-contaminated drilling wastes as sub-base material for road construction. *Waste Management & Research*, 18(5): 489-505

Veil JA (2002) Drilling waste management: past, present, and future. *SPE annual technical conference and exhibition*. Society of Petroleum Engineers.

Walter GR, Benke RR and Pickett DA (2012) Effect of biogas generation on radon emissions from landfills receiving radium-bearing waste from shale gas development. *Journal of the Air & Waste Management Association*, 62(9): 1040-1049.

Wang R, Liu J, Gao F, Zhou J and Cen K (2012) The slurrying properties of slurry fuels made of petroleum coke and petrochemical sludge. *Fuel processing technology*, 104: 57-66.

Xie L, Lv XY, Han ZJ, Ci JH, Fang CQ and Ren PG (2012) Preparation and performance of high-barrier low density polyethylene/organic montmorillonite nanocomposite. *Polymer-Plastics Technology and Engineering*, 51(12): 1251-1257.

Zhong H, Qiu Z, Huang W. and Cao J (2011) Shale inhibitive properties of polyether diamine in water-based drilling fluid. *Journal of Petroleum Science and Engineering*, 78(2): 510-515.

Zou J, Zhu H, Wang F, Sui H and Fan J (2011) Preparation of a new inorganic–organic composite flocculant used in solid–liquid separation for waste drilling fluid. *Chemical Engineering Journal* 171(1): 350-356.

Caption of Figures and Tables

Figure Captions

Fig. 1: SEM images of (a) Montmorillonite as a reference material and (b) OBM waste dry powder.

Fig. 2: SEM images of (a) neat LDPE; (b) LDPE with 2.5 wt% MMT; (c) LDPE with 5.0 wt% MMT; (d) LDPE with 7.5 wt% MMT and (e) LDPE with 10.0 wt% MMT.

Fig. 3: SEM images of (a) neat LDPE; (b) LDPE with 2.5 wt% OBM slurry; (c) LDPE with 5.0 wt% OBM slurry; (d) LDPE with 7.5 wt% OBM slurry and (e) LDPE with 10.0 wt% OBM slurry.

Fig. 4: Comparison of ATR-FTIR common scale spectra of LDPE and LDPE/MMT nanocomposites.

Fig. 5: Comparison of ATR-FTIR common scale spectra of LDPE and LDPE/OBM slurry nanocomposites

Fig.6: WAXD patterns of (a) MMT and (b) OBM waste.

Fig. 7: Different XRD patterns of LDPE and LDPE/MMT nanocomposites at (a) WAXD; (b) SAXD.

Fig. 8: Different XRD patterns of LDPE and LDPE/OBM slurry nanocomposites at (a) WAXD; (b) SAXD.

Fig. 9: DSC thermograms of OBM waste at (a) glass transition temperature (Tg); (b) melting temperature (Tm) and (c) crystallisation temperature (Tc).

Fig. 10: DSC thermograms of LDPE and LDPE/MMT nanocomposites at (a) glass transition temperature (Tg); (b) melting temperature (Tm) and (c) crystallisation temperature (Tc).

Fig. 11: DSC thermograms of LDPE and LDPE/OBM slurry nanocomposites at (a) glass transition temperature (Tg); (b) melting temperature (Tm) and (c) crystallisation temperature (Tc).

Fig. 12: TGA thermograms of OBM waste at (a) onset degradation at 5% weight loss; (b) onset degradation at 10% weight loss; (c) onset degradation at 65% weight loss and (d) residue at 1000°C.

Fig. 13: TGA thermograms of neat LDPE and LDPE/MMT nanocomposites.

Fig. 14: TGA thermograms of neat LDPE and LDPE/OBM slurry nanocomposites.

Table Captions

Table 1: EDXA of OBM waste powder, neat LDPE, LDPE/MMT and LDPE/OBM slurry nanocomposites

Table 2: XRF analysis of OBM waste powder, neat LDPE, LDPE/MMT and LDPE/OBM slurry nanocomposites

Table 3: Structural composition and thermal properties details of neat LDPE, LDPE/MMT and LDPE/OBM slurry nanocomposites

Table 4: Endothermic reactions of different clay minerals at different temperature stages at TGA (Grim and Rowland 1942)

Table 5: TGA analysis at different decomposition stages of LDPE, LDPE/MMT and LDPE/OBM slurry nanocomposites

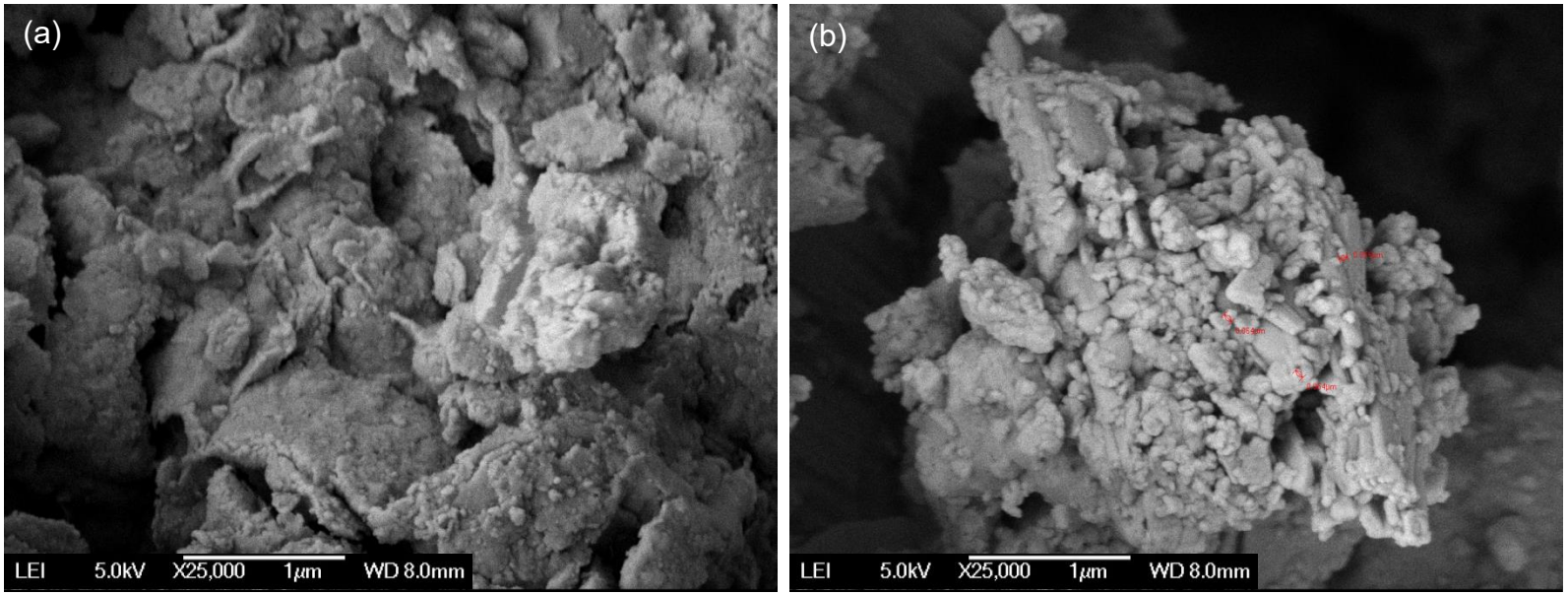

Fig. 1: SEM images of (a) Montmorillonite as a reference material and (b) OBM waste dry powder.

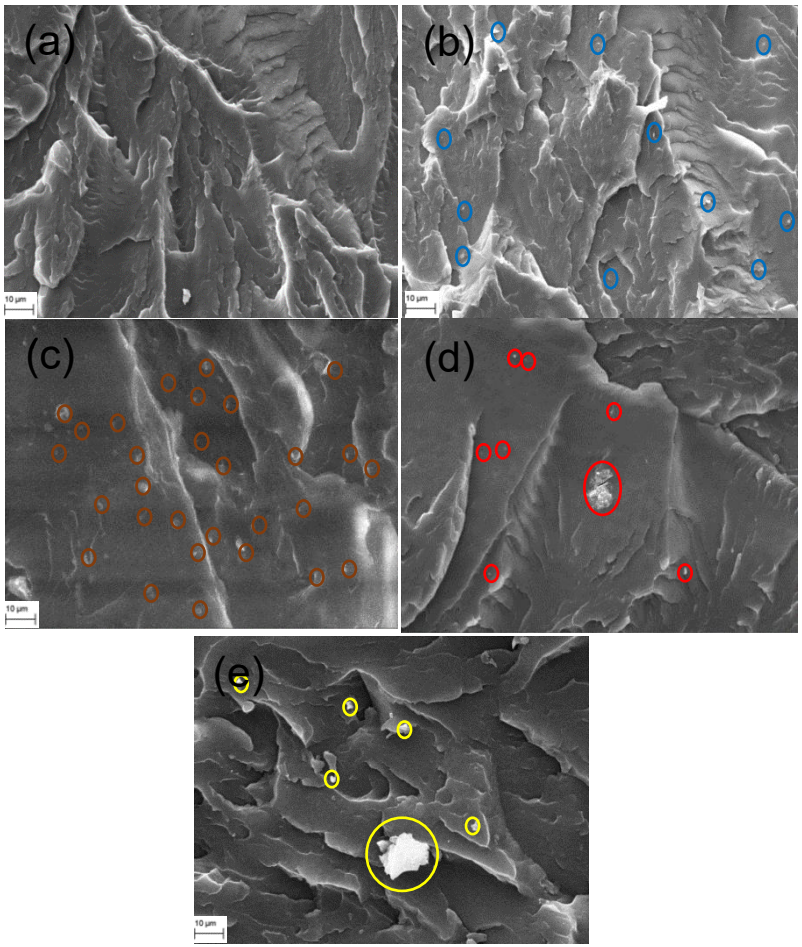

Fig. 2: SEM images of (a) neat LDPE; (b) LDPE with 2.5 wt% MMT; (c) LDPE with 5.0 wt% MMT; (d) LDPE with 7.5 wt% MMT and (e) LDPE with 10.0 wt% MMT.

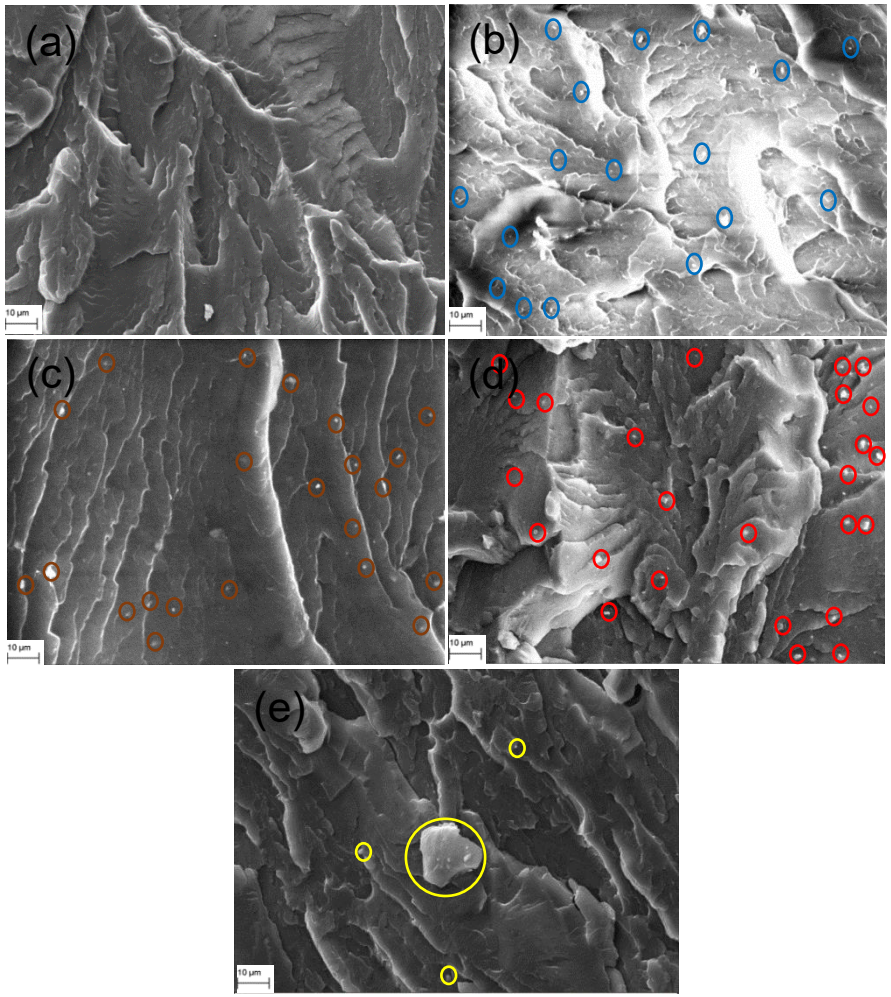

Fig. 3: SEM images of (a) neat LDPE; (b) LDPE with 2.5 wt% OBM slurry; (c) LDPE with 5.0 wt% OBM slurry; (d) LDPE with 7.5 wt% OBM slurry and (e) LDPE with 10.0 wt% OBM slurry.

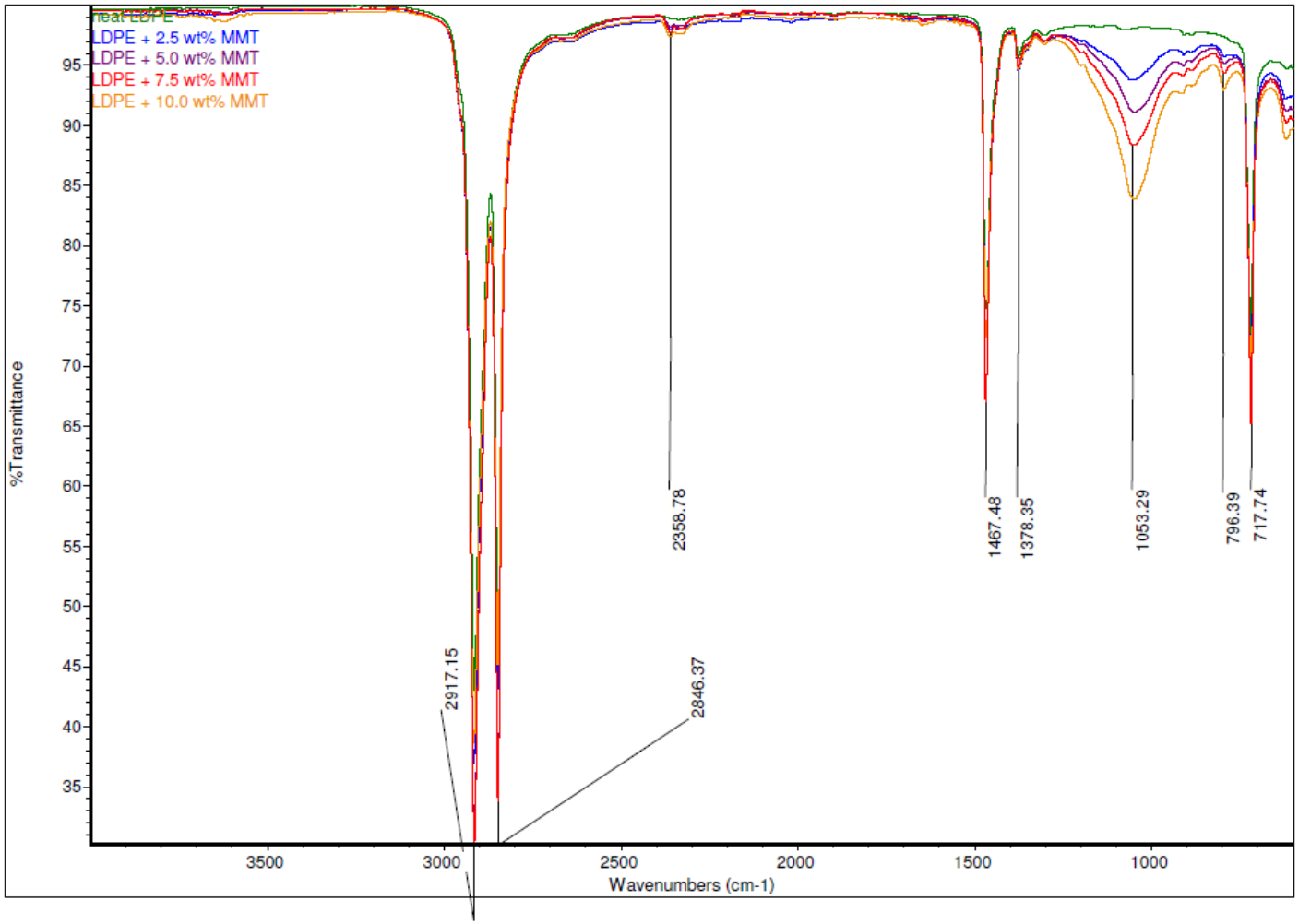

Fig. 4: Comparison of ATR-FTIR common scale spectra of LDPE and LDPE/MMT nanocomposites.

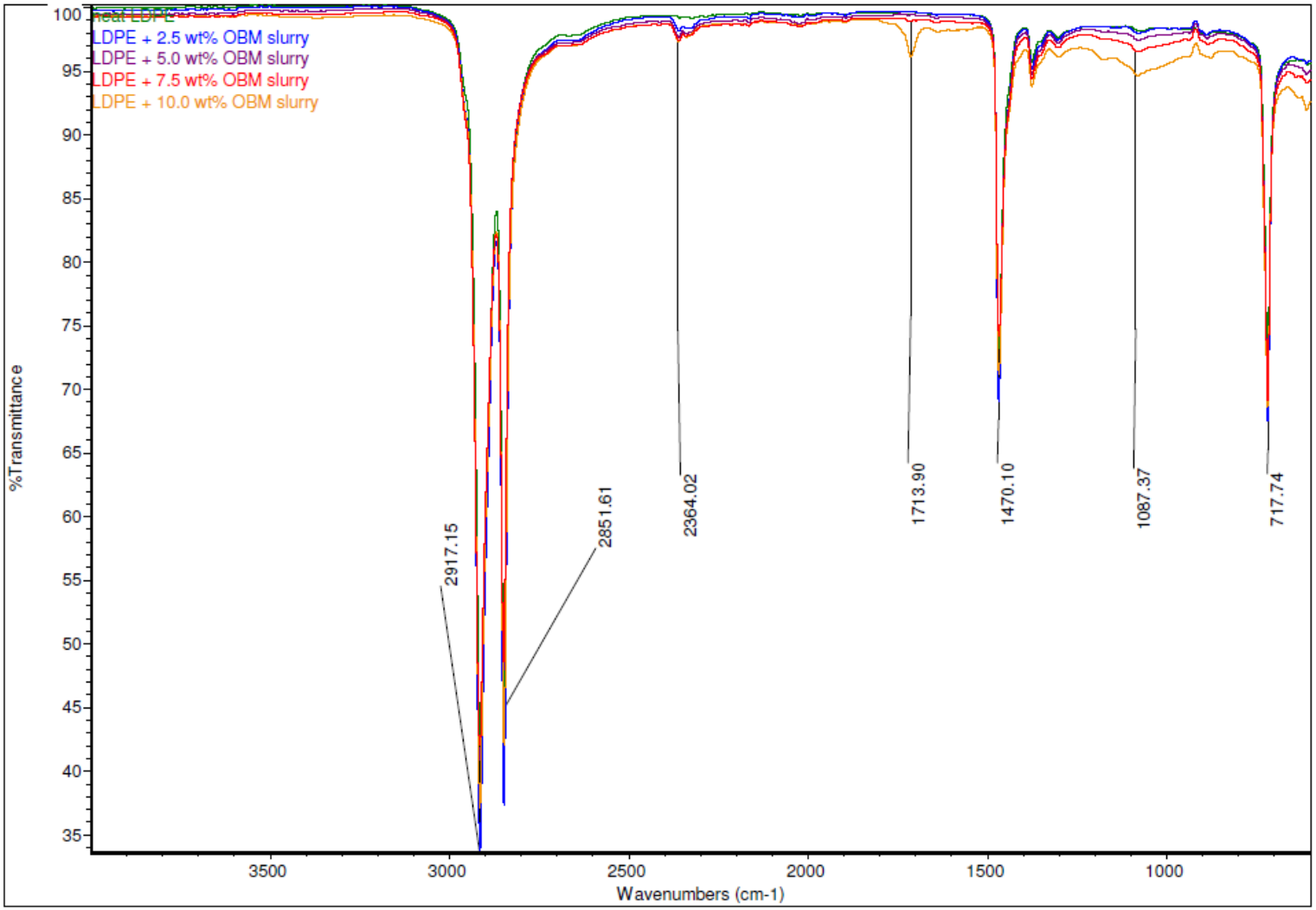

Fig. 5: Comparison of ATR-FTIR common scale spectra of LDPE and LDPE/OBM slurry nanocomposites.

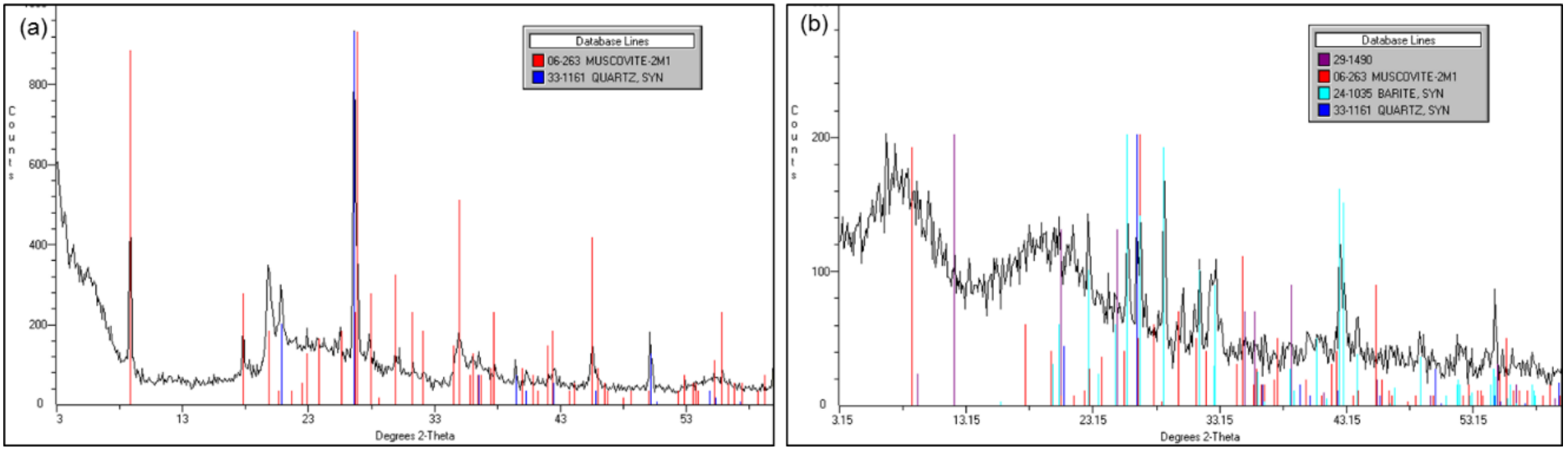

Fig.6: WAXD patterns of (a) MMT and (b) OBM waste.

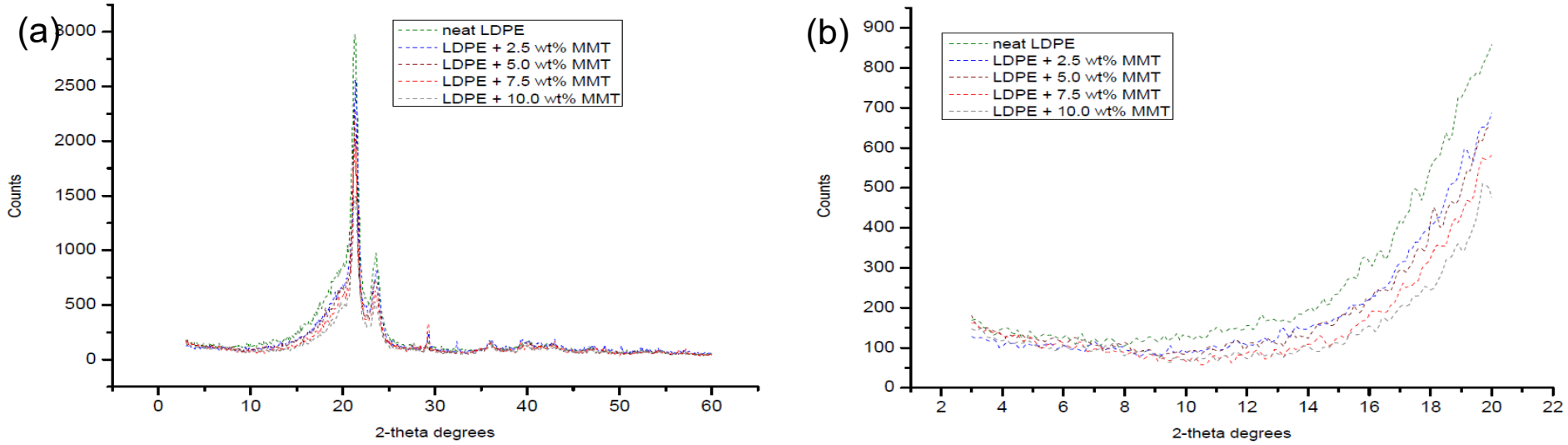

Fig. 7: Different XRD patterns of LDPE and LDPE/MMT nanocomposites at (a) WAXD; (b) SAXD.

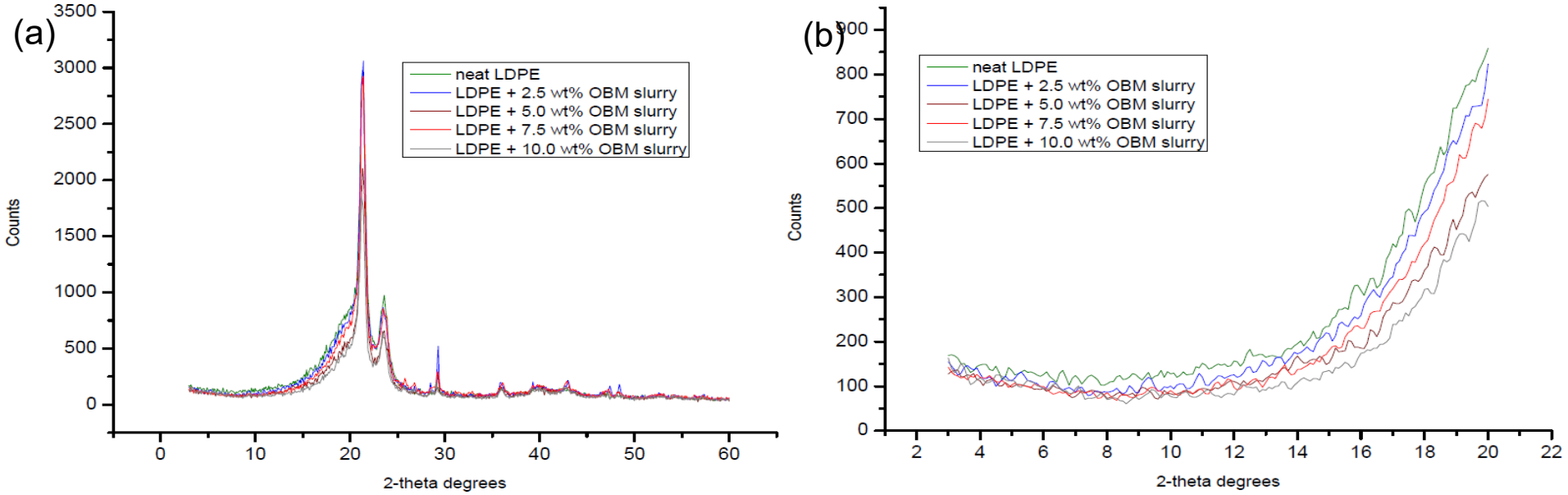

Fig. 8: Different XRD patterns of LDPE and LDPE/OBM slurry nanocomposites at (a) WAXD; (b) SAXD

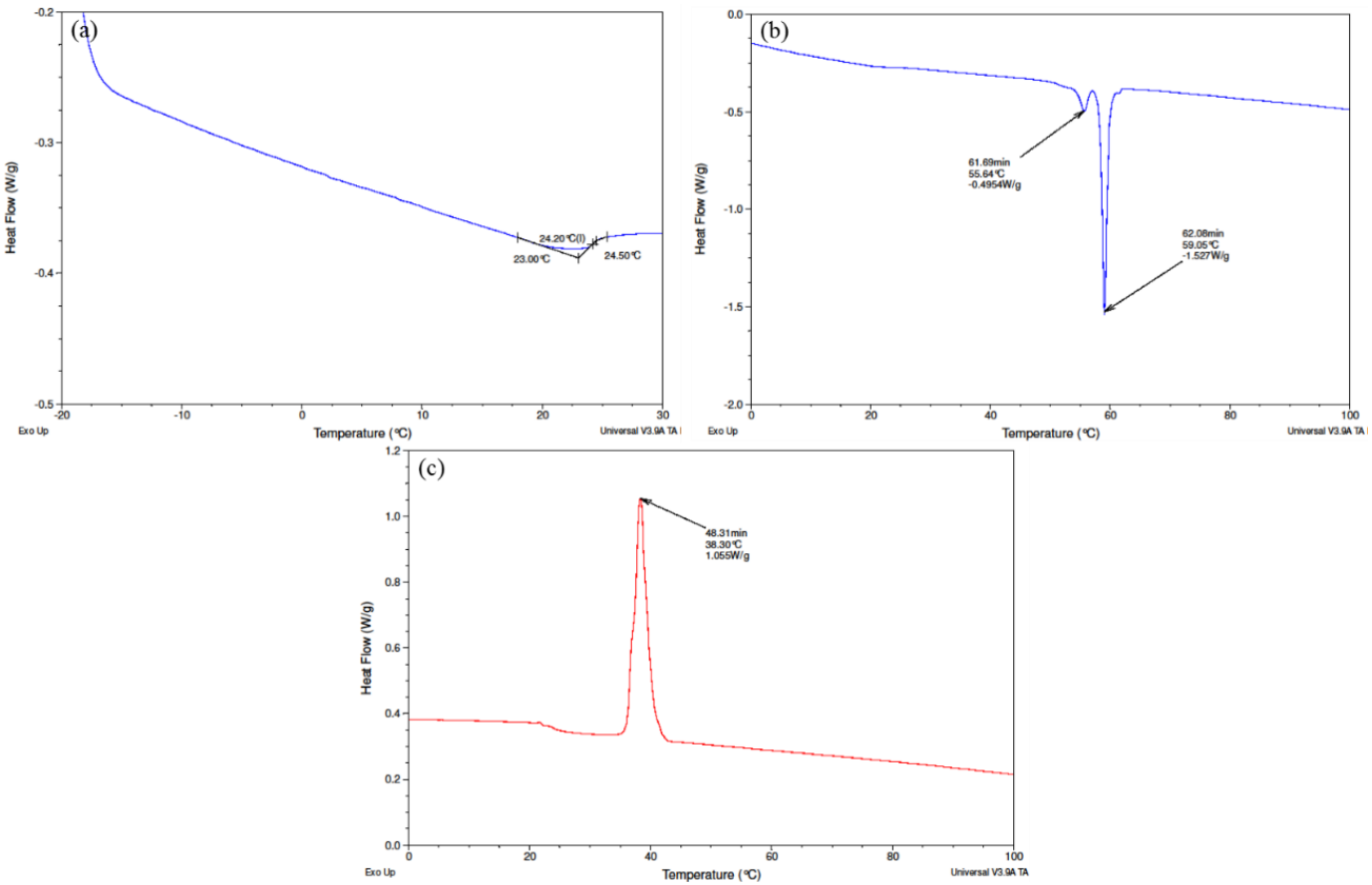

Fig. 9: DSC thermograms of OBM waste at (a) glass transition temperature (Tg); (b) melting temperature (Tm) and (c) crystallisation temperature (Tc).

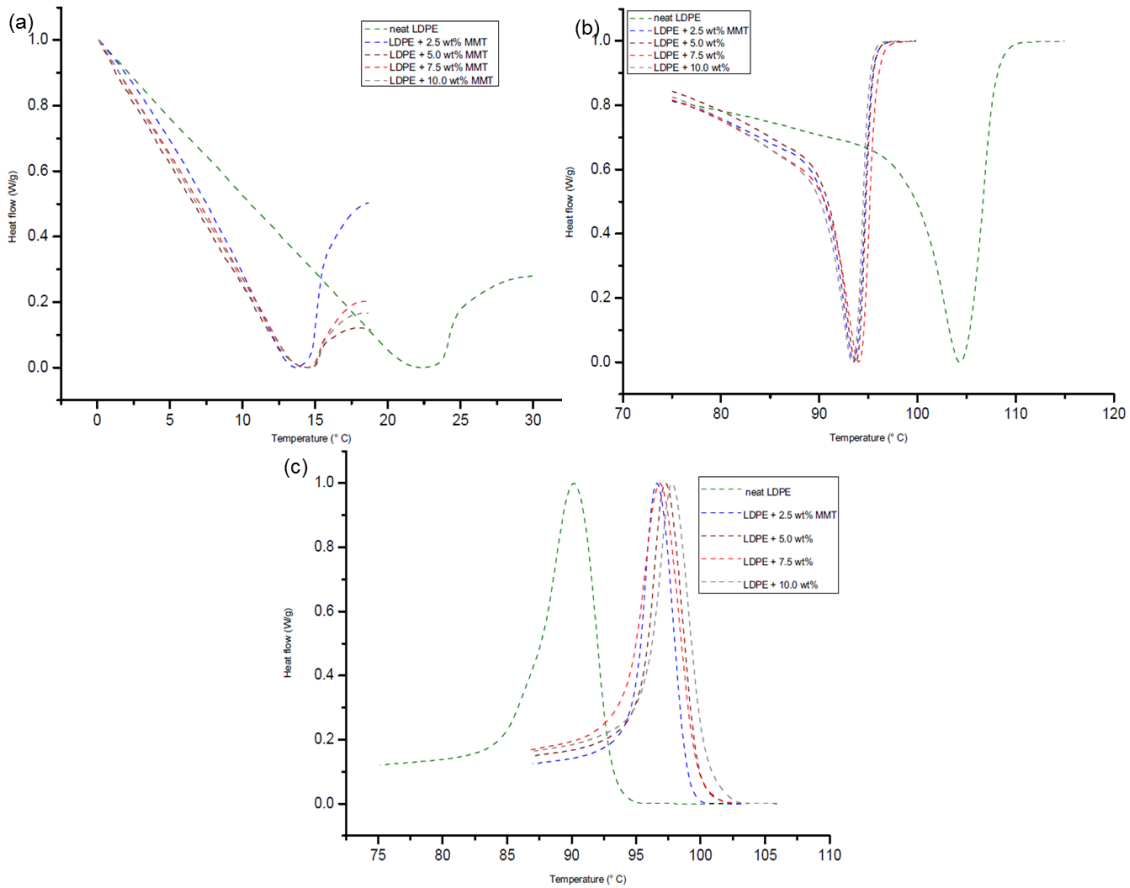

Fig. 10: DSC thermograms of LDPE and LDPE/MMT nanocomposites at (a) glass transition temperature (Tg); (b) melting temperature (Tm) and (c) crystallisation temperature (Tc).

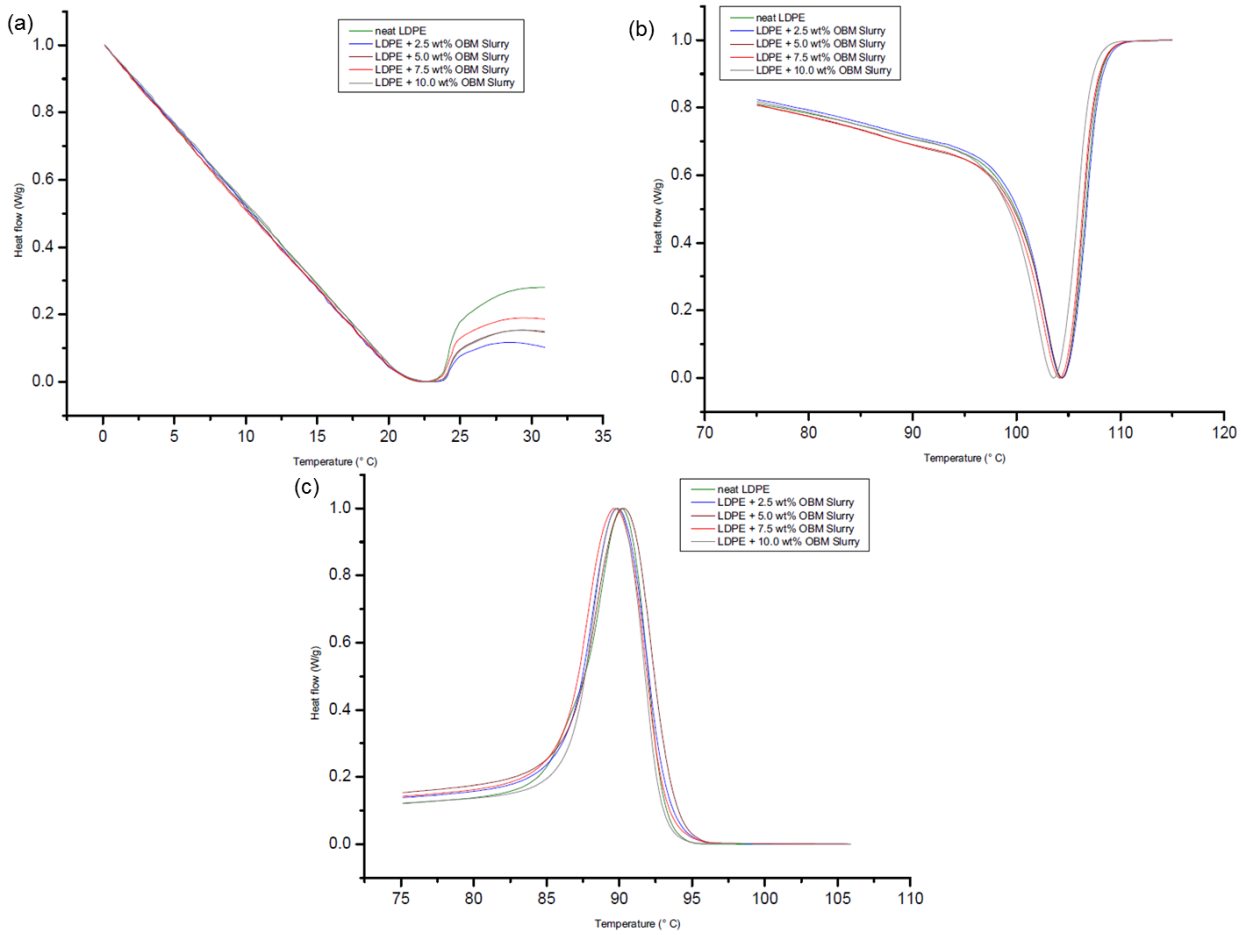

Fig. 11: DSC thermograms of LDPE and LDPE/OBM slurry nanocomposites at (a) glass transition temperature (Tg); (b) melting temperature (Tm) and (c) crystallisation temperature (Tc).

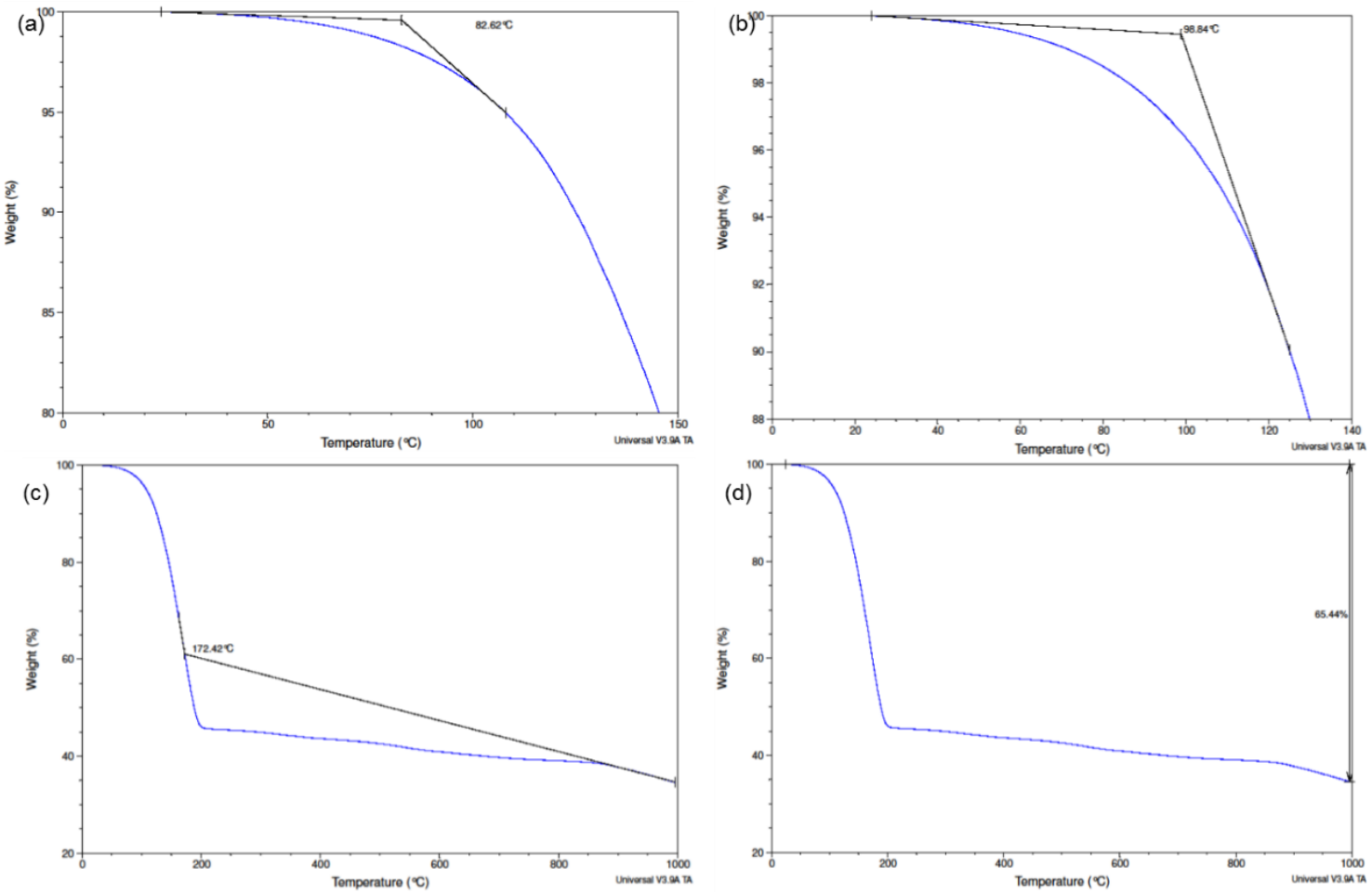

Fig. 12: TGA thermograms of OBM waste at (a) onset degradation at 5% weight loss; (b) onset degradation at 10% weight loss; (c) onset degradation at 65% weight loss and (d) residue at 1000°C.

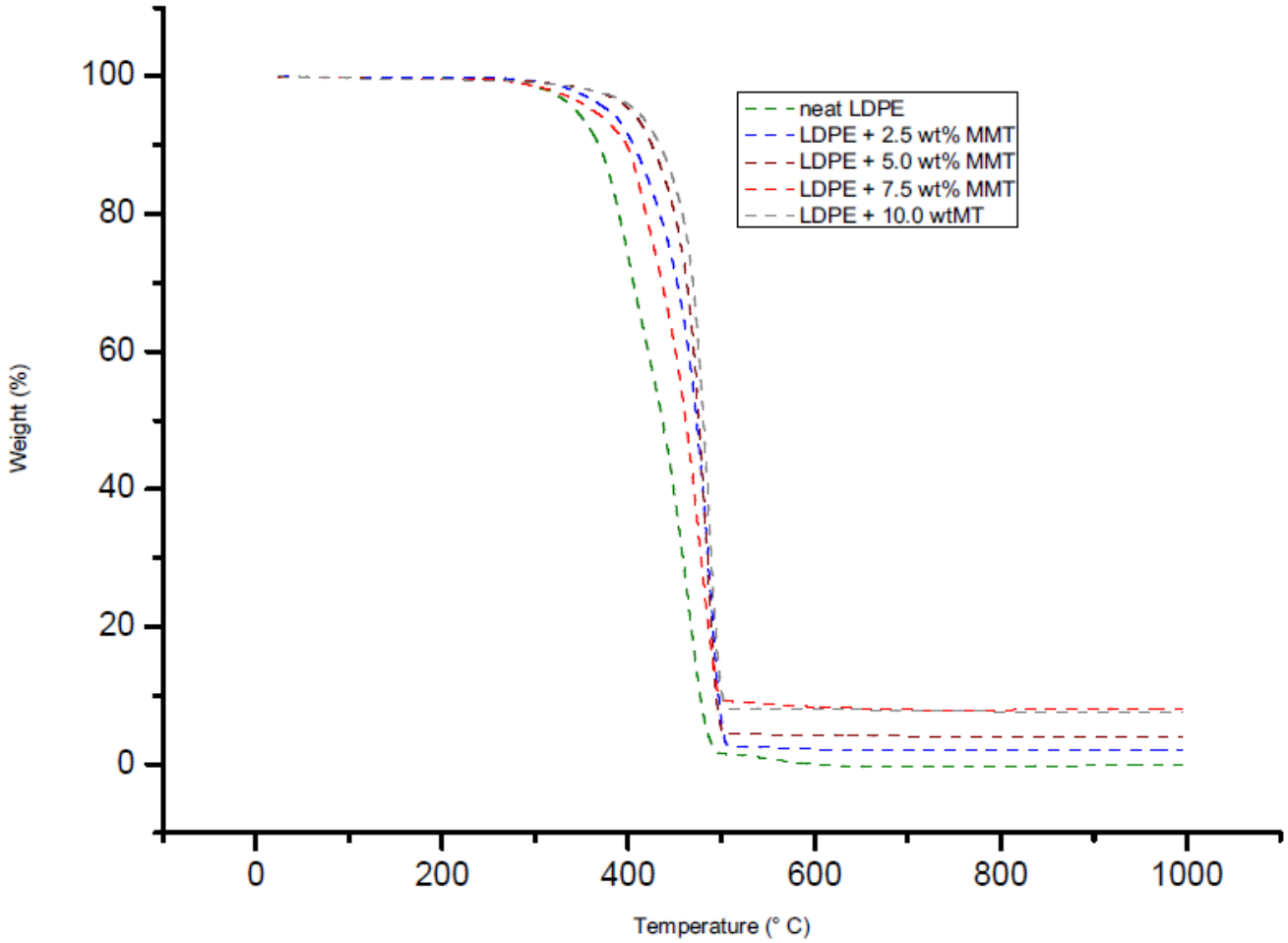

Fig. 13: TGA thermograms of neat LDPE and LDPE/MMT nanocomposites.

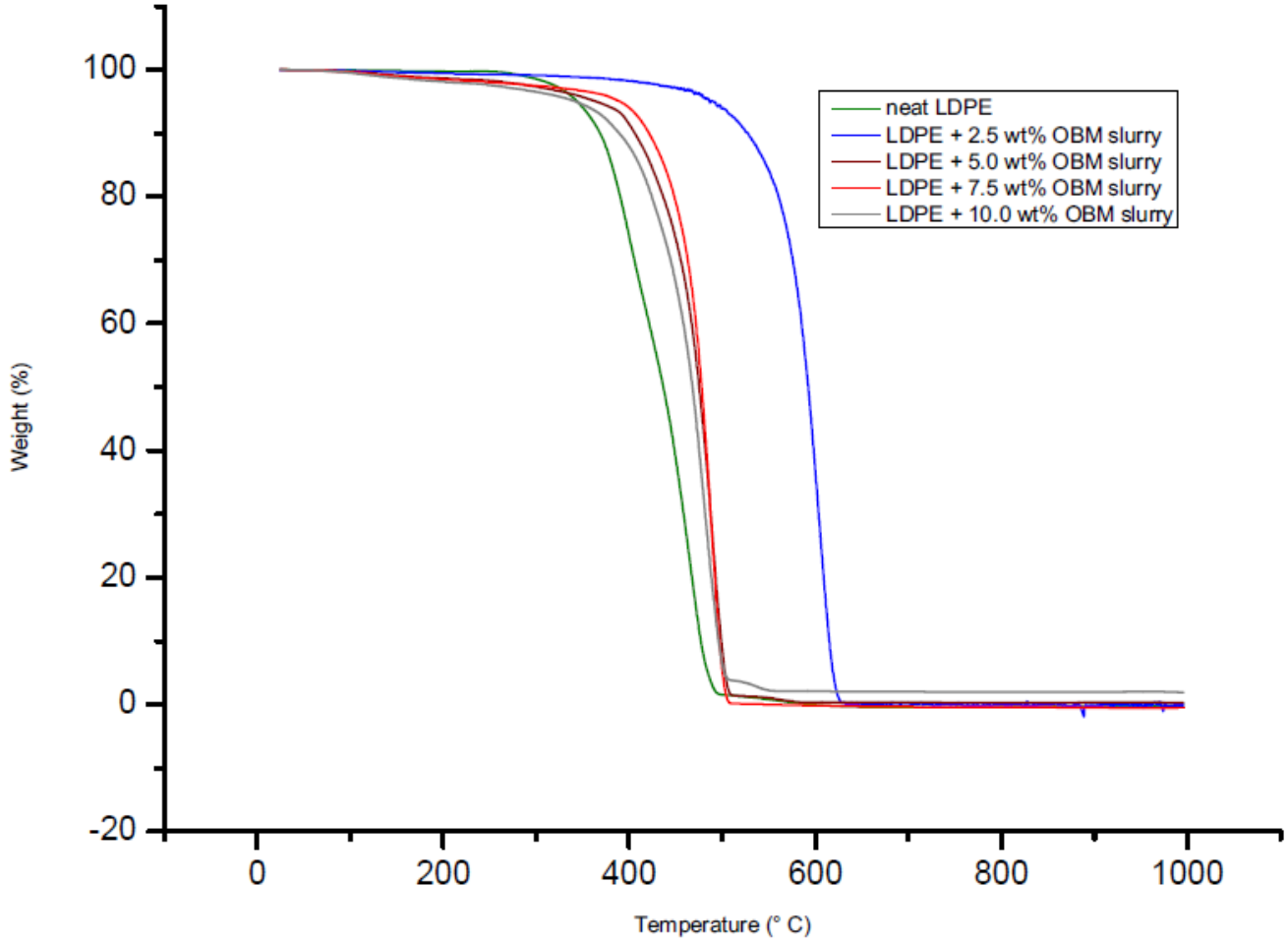

Fig. 14: TGA thermograms of neat LDPE and LDPE/OBM slurry nanocomposites.

Table 1: EDXA of OBM waste powder, neat LDPE, LDPE/MMT and LDPE/OBM slurry nanocomposites

Element	OBM clay (Dry)	Neat LDPE	LDPE + 2.5 wt% MMT	LDPE + 2.5 wt% OBM slurry	LDPE + 5.0 wt% MMT	LDPE + 5.0 wt% OBM slurry	LDPE + 7.5 wt% MMT	LDPE + 7.5 wt% OBM slurry	LDPE + 10.0 wt% MMT	LDPE + 10.0 wt% OBM slurry
C	-	98.12	96.27	96.95	94.65	97.04	91.26	97.20	88.26	97.36
O	55.3	1.88	3.13	2.79	4.56	2.58	7.47	2.44	10.12	2.20
Na	1.06	-	0.09	-	-	-	-	-	-	-
Mg	0.53	-	-	-	-	-	-	-	0.05	-
Al	2.78	-	0.12	-	0.15	0.10	0.26	0.12	0.32	0.16
Si	9.92	-	0.39	0.11	0.59	0.13	0.95	0.09	1.19	0.09
S	5.74	-	-	-	-	-	-	-	-	-
Cl	3.61	-	-	0.06	-	-	-	-	-	0.05
K	0.4	-	-	-	-	-	-	-	-	-
Ca	10.43	-	-	0.09	-	0.10	-	0.09	-	0.09
Mn	1.99	-	-	-	-	-	-	-	-	-
Fe	1.61	-	-	-	0.05	-	0.06	-	0.06	-
Ba	6.63	-	-	-	-	0.05	-	0.06	-	0.05
Totals	100	100	100	100	100	100	100	100	100	100

Table 2: XRF analysis of OBM waste powder, neat LDPE, LDPE/MMT and LDPE/OBM slurry nanocomposites

Element	OBM	neatLDPE	LDPE + 2.5 wt% MMT	LDPE + 2.5 wt% OBM slurry	LDPE + 5.0 wt% MMT	LDPE + 5.0 wt% OBM slurry	LDPE + 7.5 wt% MMT	LDPE + 7.5 wt% OBM slurry	LDPE + 10.0 wt% MMT	LDPE + 10.0 wt% OBM slurry
Sum	100.00	0.45	3.12	1.99	4.43	3.44	6.82	6.02	5.65	8.45
CaO	15.11	0.14	0.37	0.52	0.31	0.86	0.48	1.49	0.43	2.05
P_2O_5	-	0.23	0.33	0.31	0.37	0.34	0.39	0.34	0.40	0.33
Al_2O_3	6.06	-	0.17	-	0.25	-	0.42	-	0.34	-
As	0.12	-	-	-	-	-	-	-	-	-
Ba	27.41	-	-	0.22	-	0.48	-	1.07	-	1.52
Cl	3.37	-	0.03	0.08	0.03	0.13	0.04	0.22	0.03	0.27
Fe_2O_3	3.71	-	0.85	0.31	1.36	0.56	1.90	0.95	1.52	1.25
K_2O	0.65	-	-	-	-	-	-	-	-	-
MgO	0.83	-	-	-	-	-	-	-	-	-
MnO	3.35	-	-	0.25	-	0.50	-	0.94	-	1.21
Na_2O	0.57	-	-	-	-	-	-	-	-	-
SiO_2	22.18	-	1.25	0.11	1.89	0.22	3.29	0.36	2.69	0.47
SO_3	15.63	-	-	-	-	0.19	-	0.34	-	0.47
Sr	0.55	-	-	-	-	-	-	0.11	-	0.15
TiO_2	0.23	-	-	-	-	-	-	-	-	0.48
Zn	-	-	-	-	-	-	-	-	-	-
Cu	0.01	0.01	0.01	0.01	0.01	-	0.01	0.04	0.01	0.03
others	0.22	0.08	0.10	0.17	0.22	0.17	0.30	0.19	0.23	0.23

Table 3: Structural composition and thermal properties details of neat LDPE, LDPE/MMT and LDPE/OBM slurry nanocomposites

Material	% of crystallinity	RAF= 1-MAF-CF	MAF ($\Delta C_p/\Delta C_{p(am)}$)	Specific heat capacity (Cp) $JK^{-1}kg^{-1}$
Neat LDPE	16.16	0.10	0.74	3349
LDPE+2.5 wt% MMT	17.25	0.31	0.52	3063
LDPE+5.0 wt% MMT	17.98	0.30	0.52	2975
LDPE+7.5 wt% MMT	14.76	0.47	0.38	2234
LDPE+10.0 wt% MMT	12.46	0.49	0.39	2409
LDPE+2.5 wt% OBM slurry	17.17	0.33	0.50	3394
LDPE+5.0 wt% OBM slurry	13.94	0.32	0.55	2871
LDPE+7.5 wt% OBM slurry	15.65	0.17	0.67	3246
LDPE+10.0 wt% OBM slurry	13.56	0.32	0.54	2801

Table 4: Endothermic reactions of different clay minerals at different temperature stages at TGA (Grim and Rowland 1942)

Clay minerals	Reaction temperature profile
Quartz	endothermic reaction at 565°C, 870°C
Goethite	endothermic reaction at 450°C
Limonite	endothermic reaction at 350°C
Gibbsite	endothermic reaction at 350°C
Diaspore	endothermic reaction at 550°-570°C
Kaolinite	endothermic reaction at 550-600°C
Halloysite, Kaolinite and Illite	endothermic reaction at 500-650°C
Illites	endothermic reaction at 100-200°C, 500-650°C and about 900°C
Montmorillonite	endothermic reaction at 100-250°C, 600-700°C and about 900°C
Brucite	endothermic reaction at 425-475°C
Hydrated halloysite	endothermic reaction same as kaolinite with an additional reaction at 100-125°C

Table 5: TGA analysis at different decomposition stages of LDPE, LDPE/MMT and LDPE/OBM slurry nanocomposites

Material	$T_{D5\%}$ (° c)	$T_{D10\%}$ (° c)	D 1/2 Time	Residue (% wt) at 1000 °C
LDPE	381.27	407.39	45.03	0.15
LDPE+2.5 wt% MMT	329.75	368.91	45.05	1.98
LDPE+5.0 wt% MMT	373.12	399.83	45.16	3.99
LDPE+7.5 wt% MMT	316.85	350.93	44.06	7.93
LDPE+10.0 wt% MMT	373.81	401.36	45.84	7.65
LDPE+2.5 wt% OBM slurry	366.90	386.67	44.59	0.20
LDPE+5.0 wt% OBM slurry	370.09	365.39	45.44	0.37
LDPE+7.5 wt% OBM slurry	327.70	383.26	45.59	0.40
LDPE+10.0 wt% OBM slurry	350.07	333.77	44.64	1.97